

# Spectroscopy of Rb<sub>2</sub> dimers in solid <sup>4</sup>He

P. Moroshkin,\* A. Hofer, S. Ulzega, and A. Weis  
 Département de Physique, Université de Fribourg,  
 Chemin du Musée 3, 1700 Fribourg, Switzerland†  
 (Dated: July 10, 2018)

We present experimental and theoretical studies of the absorption, emission and photodissociation spectra of Rb<sub>2</sub> molecules in solid helium. We have identified 11 absorption bands of Rb<sub>2</sub>. All laser-excited molecular states are quenched by the interaction with the He matrix. The quenching results in efficient population of a metastable (1)<sup>3</sup>Π<sub>u</sub> state, which emits fluorescence at 1042 nm. In order to explain the fluorescence at the forbidden transition and its time dependence we propose a new molecular exciplex Rb<sub>2</sub>(<sup>3</sup>Π<sub>u</sub>)He<sub>2</sub>. We have also found evidence for the formation of diatomic bubble states following photodissociation of Rb<sub>2</sub>.

PACS numbers: 33.20.-t, 33.50.-j, 33.80.Gj, 67.80.Mg, 67.80.-s

## I. INTRODUCTION

The spectroscopy of alkali dimers, in particular of the Rb<sub>2</sub> molecule is a well established area of research [1, 2, 3, 4]. Recently it has attracted renewed attention in connection with the creation of ultracold molecules via the photoassociation of ultracold atoms in magneto-optical traps [5, 6]. In such experiments the ultracold molecules are usually produced in their lowest triplet state (*a*<sup>3</sup>Σ), and their transfer into the zero-vibration singlet ground state *X*<sup>1</sup>Σ remains a major problem [7, 8, 9]. Another recently developed technique [10, 11, 12, 13] involves the attachment of several alkali atoms to a superfluid helium nano-droplet, where they cool down to 0.38 K and may form a dimer. The energy released in the formation of a strongly bound molecule in its singlet ground state usually results in the complete evaporation of the nano-droplet, therefore only weakly bound triplet states could be observed in most of these studies. There have been a few reports on alkali dimers in cryogenic rare-gas matrices. Takahashi *et. al.* [14] observed emission of Na<sub>2</sub> molecules in superfluid helium, and some absorption bands of Li<sub>2</sub> and Na<sub>2</sub> in solid xenon were reported in [15]. Theoretical studies were reported for Na<sub>2</sub> in solid argon [16, 17].

In our earlier publications, the spectroscopy of Cs and Rb atoms in solid helium has been well established [18, 19, 20, 21]. The absorption of laser radiation at the wavelengths of the Cs *D*<sub>1</sub> and *D*<sub>2</sub> transitions, blueshifted by the interaction with the He matrix, induces fluorescence on the atomic *D*<sub>1</sub> line and emission bands from bound-free transitions in Cs\*He<sub>2</sub> and Cs\*He<sub>7</sub> exciplexes. Fluorescence from Rb atoms in solid helium is quenched by the interaction with the matrix [22]. The quenching is attributed to the very fast formation of Rb\*He<sub>*N*</sub> exciplexes. A weak absorption on the Rb *D*<sub>1</sub> transition at 760 nm has been detected in a transmission experiment

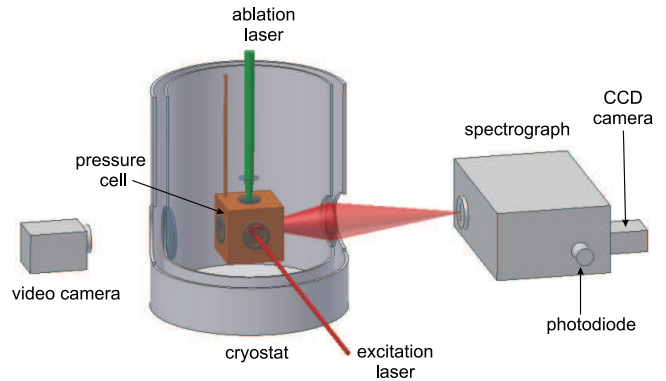


FIG. 1: Vertical section through the helium bath cryostat showing the pressure cell. A pulsed focused laser beam (532 nm) from the top is used for the implantation, and a non-focused horizontal laser beam is used for the excitation of the implanted atoms/molecules. The video camera is used to monitor crystal growth and the implantation process.

[20]. Only recently [21] a weak fluorescence from the Rb *D*<sub>1</sub> and *D*<sub>2</sub> transitions was obtained in solid He, together with the emission of Rb\*He<sub>*N*</sub> exciplexes. No fluorescence from nor absorption by Rb<sub>2</sub> molecules in bulk solid or liquid He has been reported so far. Here we present the first experimental study of Rb<sub>2</sub> dimers in solid helium.

## II. EXPERIMENT

### A. Experimental setup

The experimental setup is illustrated in Fig. 1. A solid <sup>4</sup>He matrix doped with Rb atoms was produced by the technique described in our earlier papers [19, 23]. The measurements were performed in the hcp and bcc crystalline phases of solid <sup>4</sup>He in the pressure range of 27 – 36 bar, at a temperature of 1.5 K. The sample was produced in a helium pressure cell immersed in superfluid helium cooled by pumping on the helium bath. Windows

\*peter.moroshkin@unifr.ch  
 †www.unifr.ch/physics/frap/

provide optical access from three orthogonal directions. A helium crystal is grown inside the pressure cell, by condensing and then solidifying pressurized helium gas from an external reservoir. The helium host matrix is then doped with rubidium atoms, as shown in Fig. 1, by means of laser ablation with the second harmonic of a pulsed frequency-doubled Nd:YAG-laser beam (or the signal beam of the OPO described below) focused onto a solid target containing pure natural Rb or a Rb-Cs mixture.

We have studied the absorption spectrum of the sample in the range of 400-1000 nm. In order to cover such a broad range, three sources of coherent radiation were used: (i) the signal beam from an optical parametric oscillator (OPO, OPTA GmbH model BBO-355-vis/IR), pumped by the third harmonic (354 nm) of a pulsed Nd:YAG laser for 400-700 nm; (ii) the idler beam of the same OPO for 780-1000 nm, and (iii) a tunable cw Ti:Sa laser pumped by a Nd:YVO<sub>3</sub> laser for 720-780 nm. The excitation laser beams (ii) and (iii) cross the pressure cell in a horizontal direction, passing through the volume of maximal doping. The beam (i) illuminates the sample from the top of the cryostat. In this configuration the signal beam of the OPO (pulse energy of 2 mJ, pulse width of 5 ns, wavelength in the range of 500-670 nm) can also be used as implantation laser.

Fluorescence light from the sample volume (approx. 3 mm<sup>3</sup>) is collected by a lens located in the cryostat and then analyzed by a grating spectrograph (Oriel, model MS257) with a resolution of 2 nm equipped with a CCD camera. In addition to spectral measurements we also performed time-resolved studies of the molecular fluorescence, for which we used a Si photodiode mounted after a second output slit of the spectrograph. The time-resolution of this system is limited by the 100 kHz bandwidth of the preamplifier.

## B. Observed emission spectra

The fluorescence spectrum observed in experiments with a crystal doped from a solid Rb target contains features which can be associated with atomic Rb, with Rb<sub>2</sub> dimers and with Rb\*He<sub>N</sub> exciplexes (Fig. 2). Recently we have done a detailed spectroscopic study of the Rb-He exciplexes [21]. We restrict the present discussion to Rb and Rb<sub>2</sub>. A typical emission spectrum obtained under excitation at 570 nm is shown in Fig. 2, in which one distinguishes three spectral features. The two components of the narrow doublet at 780 nm are easily identified as the *D*<sub>1</sub> and *D*<sub>2</sub> emission lines of atomic Rb. They are separated by 14 nm, which corresponds to the fine-structure splitting of the Rb 5*P*<sub>*J*</sub> states in solid helium. Both components of the doublet are strongly broadened and blueshifted with respect to the free Rb atom due to the interaction with the surrounding He. Both the shift and the spectral width depend on the He pressure. The intensity of these two lines is orders of magnitude lower

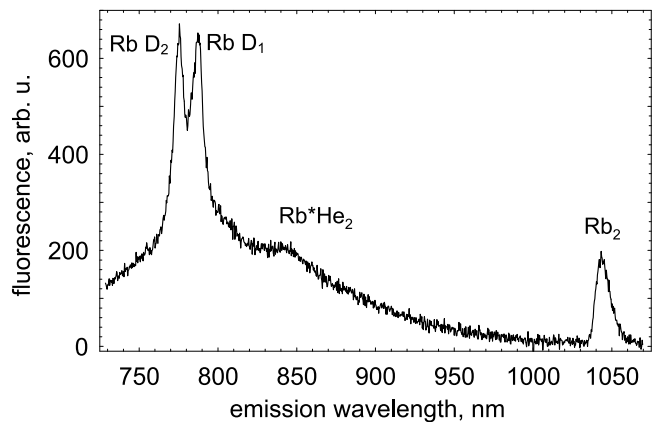


FIG. 2: Measured emission spectrum from Rb implanted in solid helium ( $T=1.5$  K,  $p=31$  bar). Excitation by the focused signal beam of the OPO at 570 nm.

than the intensity of the *D*<sub>1</sub> line of Cs recorded under similar conditions [19]. In a previous study [20] the *D*<sub>1</sub> line of Rb was excited by a cw Ti:Sa laser in an absorption experiment at 760 nm, but fluorescence was overlooked in that experiment, probably because of the strong intensity of scattered laser radiation in this part of the spectrum. We attribute the central spectral feature of Fig. 2 to Rb\*He<sub>2</sub> exciplexes, formed by the atomic 5*P* states as discussed in detail elsewhere [21]. The rightmost spectral feature at 1042 nm originates from the Rb<sub>2</sub> dimer. It is the only molecular band that could be observed in the fluorescence spectrum in the range of 500-1600 nm, when exciting the sample in the range of 450-900 nm.

## C. Excitation spectra

The molecular emission at 1042 nm can be excited on a number of resonant absorption bands. The excitation spectrum of the 1042 nm emission is shown in Fig. 3(a). The rightmost band centered at 842 nm (feature "a") is the strongest band observed in the present experiments. The band at 740 nm (labelled "b") overlaps with the *D*<sub>2</sub> absorption line of atomic Rb. As a rule, the signal is much larger when the beam is focused and illuminates the sample in the vertical direction. However, some of the other bands with maxima at 650, 580, 525, and 445 nm could even be observed with a non-focused beam. In addition, the blue wing of the band at 650 nm has a shoulder (labelled "d"), which can be interpreted as a weaker band partially overlapping with the 650 nm band. At higher helium pressures this band shifts towards the blue at a faster rate than the stronger band. At 35 bar its maximum is at 625 nm and the two bands become resolved.

The fact that the emission peak at 1042 nm appears under excitation at very different wavelengths and that no other molecular emission is observed suggests that all molecular excited states are quenched by the interac-

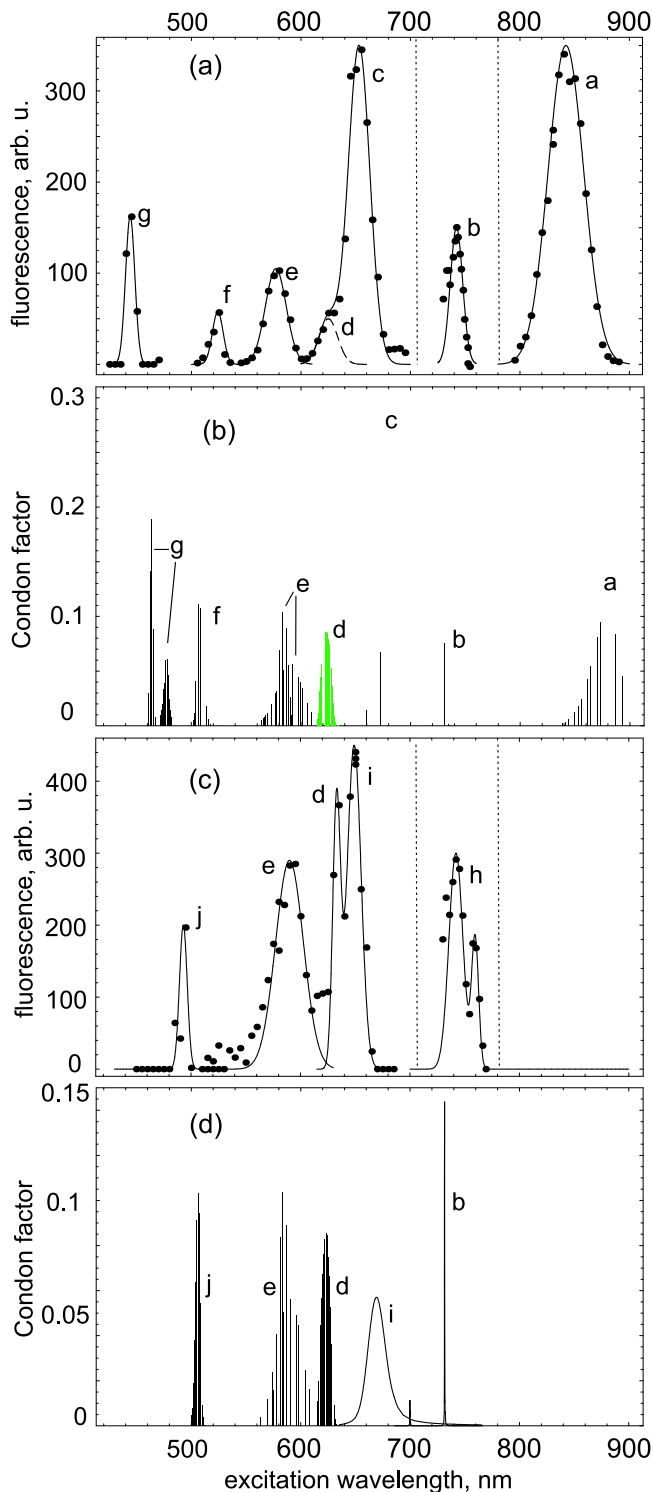


FIG. 3: (a) measured excitation spectrum of the molecular fluorescence at 1042 nm, (c) measured photodissociation spectrum of the Rb dimer (detected via the atomic Rb fluorescence at 780 nm). (b), (d) are calculated Condon factors for the transitions from the  $X^1\Sigma_g$  and  $(1)^3\Sigma_u$  states populating the  $(1)^3\Pi_u$  state (b) and the atomic  $5P_{1/2}$  state (d). Experimental data are shown as points, and the solid lines are fitted Gaussians. The assignment of all peaks is given in Table III C and in the text of Sec. III. The dotted vertical lines mark the spectral regions covered by the 3 excitation sources described in the text. The vertical scales differ for the different intervals.

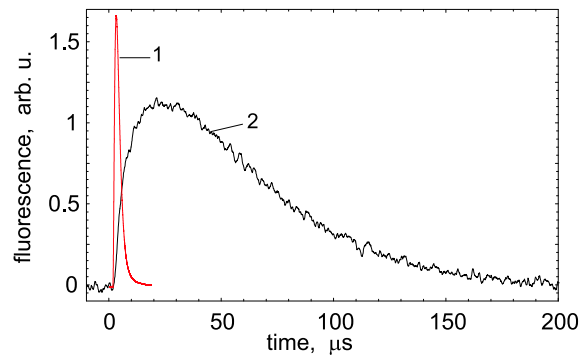


FIG. 4: Measured pulse-shapes of the molecular fluorescence at 1042 nm (curve 2) and scattered of laser light at 842 nm (curve 1). The actual width of the laser pulse (5 ns) is not resolved so that curve 1 represents the time resolution of the photodetector.

tion with the helium matrix. The excitation of any state seems to be followed by very fast radiationless or far infrared transitions to a low-lying state which decays by emitting 1042 nm light.

Fig. 3(c) shows the excitation spectrum for atomic emission on the Rb  $D_1/D_2$  doublet (actually the detection spectrograph was set to 780 nm, which corresponds to  $D_1$  emission). The features "j", "e", "d", and "i" show that atomic emission can not only be excited by absorption at the atomic resonance lines (740 and 760 nm respectively), but also at 650, 580, and 495 nm. We assign these bands to absorption by molecular state(s) of Rb<sub>2</sub> which dissociate into one ground-state and one excited state atom.

#### D. Time resolved fluorescence

We measured the time dependence of the molecular fluorescence following pulsed excitation at selected excitation and emission wavelengths. A characteristic fluorescence pulse shape is shown in Fig. 4. The atomic and exciplex emission decay-times are too short to be resolved by our detection system. Both channels yield a fluorescence pulse which coincides with that of the scattered laser light (curve 1 in Fig. 4) and thus reflects the time resolution (FWHM = 3  $\mu$ s) of the detector. This is consistent with other studies of atomic Rb and Cs in liquid He [22], and our own (unpublished) results on Cs in solid He in which atomic lifetimes on the order of a few 10 ns were observed. The molecular fluorescence at 1042 nm shows an exponential decay with a characteristic time of 45  $\mu$ s that is well resolved (curve 2 in Fig. 4). The fluorescence pulse shows also an intriguing finite rise-time of approximately 15  $\mu$ s. Pulse shapes with identical decay and rise-times could be measured when exciting either at 840 or at 650 nm.

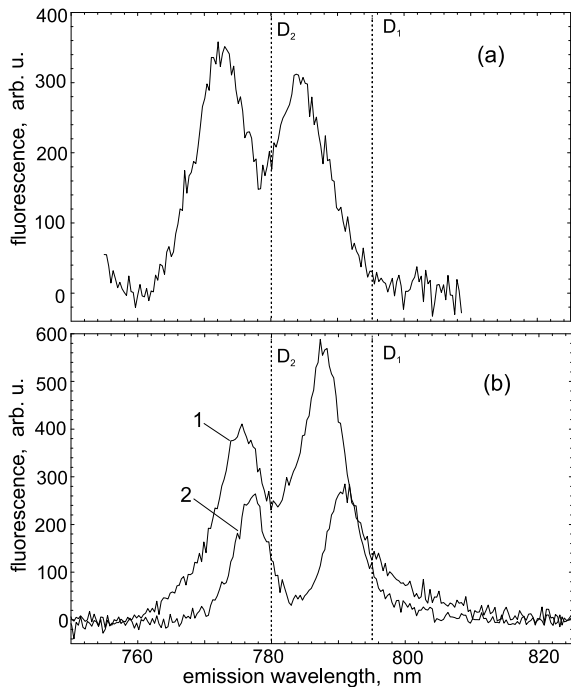


FIG. 5: Measured emission spectrum of atomic Rb produced by excitation of the atomic  $5P_{3/2}$  state at 740 nm (a) and by photodissociation of  $Rb_2$  following excitation at 650 nm (b): curve 1 - hcp phase at  $p = 30$  bar, curve 2 - during the solid-liquid phase transition at  $p = 26.4$  bar. Vertical dashed lines mark the wavelengths of the free atomic  $D_1$  and  $D_2$  lines at 795 and 780 nm.

### E. Emission spectra at the phase transition

We have performed experiments at different helium pressures in the range of 26-36 bar. At 1.5 K, two phase transitions occur within this range [24]. The solidification of superfluid He at 26.4 bar produces first a body-centered cubic (bcc) crystalline structure, and then a hexagonal close-packed (hcp) structure at 26.8 bar. The standard implantation procedure described above produces the best results, i.e., the largest density of implanted species and hence of spectroscopic signals when applied at 29.5 bar in the hcp crystal. By releasing the pressure after the doping process to below 27 bar we were able to observe molecular and atomic fluorescence in the bcc phase and even during the transition to the liquid phase.

When atomic Rb in a hcp crystal at 30 bar is excited at 740 nm the  $D_1/D_2$  fluorescence spectrum (Fig. 5(a)) is blue-shifted by approximately 10 nm and strongly broadened with respect to the free atomic lines. When the same fluorescing transitions are observed after photodissociation of  $Rb_2$  at 650 nm under otherwise identical conditions the emission lines shown as curve 1 in Fig. 5(b) are observed. The spectrum shows a reduced blue shift of approximately 7 nm. These fluorescence spectra exhibit interesting features, when recorded during the melting

process. The blueshift and the intensity of the fluorescence following absorption on the photodissociating band at 650 nm decrease with decreasing He pressure, similar to the behavior observed on the atomic fluorescence of Cs (excited on the atomic  $D_1$  line) in solid He [19]. However, unlike the observation of the purely atomic process in cesium-doped helium, the intensity rises again when the (photodissociation-induced) fluorescence is recorded during the phase transition to the liquid. The fluorescence recorded under the latter conditions is shown as curve 2 in Fig. 5(b). One sees that the spectral width of each component of the atomic fluorescence doublet (curve 2) coming from that structure is smaller and that their intensity ratio differs from the one observed in hcp helium (curve 1). The blueshift of both spectral lines under those conditions is only 4.0 nm, much smaller than in solid He, but also significantly smaller than in pressurized (25 bar) superfluid He [25], when excited at the atomic  $D_1$  line (760 nm). We could not observe any fluorescence after the complete melting of the crystal.

The molecular fluorescence band at 1040 nm (excited at 650 nm) exhibits a qualitatively different behavior at the same phase transition. The spectral position and the width of the band do not show a measurable pressure dependence and the intensity quickly vanishes at the transition from the bcc phase to the liquid. We could not detect any molecular emission induced by excitation at 650 nm, under the same conditions in which curve 2 of Fig. 5(b) was obtained.

We have performed the same measurements when the sample is irradiated with 580 nm light. Here the behavior is again quite different. The atomic fluorescence disappears already at the beginning of the bcc to liquid phase transition, while, at the same time, the molecular fluorescence can be observed until the complete melting. This interesting phenomenon will be discussed below.

## III. THEORETICAL MODEL

The dimer  $Rb_2$  is the best candidate for describing most of the observed spectral lines described above, and we will substantiate this assignment by discussing its absorption and fluorescence spectra in detail.

### A. Molecular potentials

Theoretical *ab initio* potential curves of the  $Rb_2$  molecule are available in the literature [26, 27]. The potentials from [26] are shown in Fig. 6. The ground state of  $Rb_2$  has two components: a deeply bound (covalent) singlet state  $X^1\Sigma_g$  and a weakly bound (van der Waals) triplet state  $(1)^3\Sigma_u$ .

The wavefunctions of the molecule's oscillations depend on a single parameter  $r$ , the internuclear separation in the diatomic molecule, and can be found by solving the

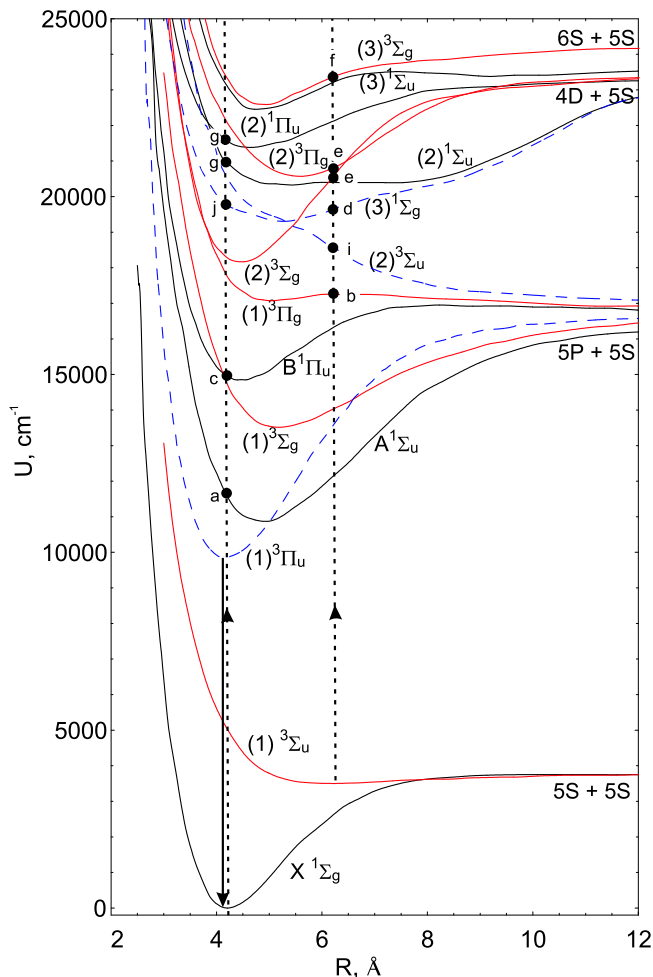


FIG. 6: Theoretical *ab initio* potential curves of the  $\text{Rb}_2$  molecule, from [26]. Solid lines - states connected by the allowed transitions to the one of two ground-states; dashed lines - states without the allowed transition to the ground-state (only the states discussed in this work are shown). Two vertical dashed lines mark the vertical transitions from the singlet and triplet ground-state at 4.2 and 6.2 Å, and the vertical solid arrow indicates the emission from the metastable state.

one-dimensional Schrödinger equation

$$-\frac{\hbar^2}{2m} \frac{d^2 \Psi_\alpha^{(v)}}{dr^2} + V_\alpha(r) \Psi_\alpha^{(v)} = \omega_v \Psi_\alpha^{(v)}, \quad (1)$$

for the corresponding potential  $V_\alpha(r)$ , where  $\omega_v$  is the eigenenergy of the vibrational state  $v$ .

The transition probabilities between vibrational states of a given electronic transition are given by the Franck-Condon factors, i.e., the overlap integrals between the wavefunctions of excited ( $\Psi_e$ ) and ground ( $\Psi_g$ ) states. There is an important simplification resulting from the fact that at the temperature of our experiments (1.5 K) only the lowest molecular vibration states are populated. Therefore the absorption spectrum consists only of transitions from the  $v = 0$  vibration level in the electronic

ground state to all vibrational levels  $v'$  in the excited state, for which the Franck-Condon factors are given by

$$F_{exc}^{(v')} = \left| \int \Psi_g^{(0)}(r) \Psi_e^{(v')}(r) dr \right|^2, v' = 0, 1, 2, \dots \quad (2)$$

In the same way, the emission spectrum consists of transitions from the  $v' = 0$  vibration level in the electronic excited state to all vibrational levels  $v$  in the ground state.

$$F_{emis}^{(v)} = \left| \int \Psi_g^{(v)}(r) \Psi_e^{(0)}(r) dr \right|^2, v = 0, 1, 2, \dots \quad (3)$$

When calculating the Franck-Condon factors one has to take into account the selection rules, which allow only transitions between terms of the same multiplicity, while transitions between singlet and triplet states are forbidden. In most spectroscopic experiments [3], the alkali dimers are produced in a hot and dense atomic vapor in which only the deeply bound  $X^1\Sigma_g$  state is populated. Therefore only the transitions between singlet states have been studied in detail and the corresponding potential curves evaluated. As for the triplet states, the available potential curves are obtained mainly from *ab initio* calculations.

## B. Emission spectrum

The long decay-time of the molecular fluorescence suggests that it originates from a metastable state and that the corresponding transition is forbidden in the free molecule. Inspection of the potential energy diagram in Fig. 6 reveals the  $(1)^3\Pi_u$  state to be a good candidate for the excited state of the fluorescing transition. It is the lowest lying excited state of the molecule, and it can be populated by a cascade of radiationless transitions following laser excitation to any other higher lying state. In the free molecule the transition to the singlet ground-state  $X^1\Sigma_g$  is forbidden by multiplicity and the triplet-triplet transition to the  $(1)^3\Sigma_u$  state by parity. The absence of fluorescence from other excited states suggests that in solid He these states are quickly quenched and that all excited population is collected in the long-lived  $(1)^3\Pi_u$  state, which finally decays towards the  $X^1\Sigma_g$  ground-state. A similar effect was reported in spectroscopic studies of  $\text{Hg}_2$  dimers in a cryogenic Ar matrix [28], where only the emission from the metastable  $A0_g^+$  state was observed under excitation on four different allowed transitions.

The potentials in Fig. 6 show that the minimum of the  $(1)^3\Pi_u$  potential lies almost at the same internuclear distance as the minimum of the ground state. The overlap integral between the lowest vibrational states  $v' = v = 0$  is therefore exceptionally large and quickly vanishes with increasing  $v'$ . In fact only  $0 \rightarrow 0$  and  $0 \rightarrow 1$  transitions produce non-negligible contributions to the spectrum. In

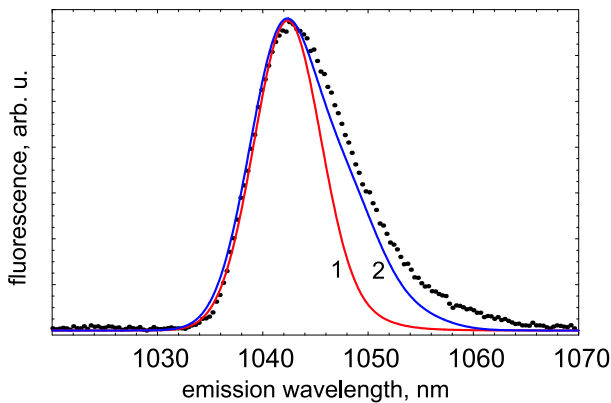


FIG. 7: Experimental (points) and calculated (solid curves) emission spectra of  $(1)^3\Pi_u \rightarrow X^1\Sigma_g$  transition in  $\text{Rb}_2$ . Curve 1 was obtained by shifting the calculated curve by 20 nm to the red. Curve 2 is obtained by shifting the excited state potential curve by  $0.12 \text{ \AA}$  towards larger interatomic distances, and then shifting again the calculated spectrum by 20 nm to the red.

order to model the observed emission band, we represent these two components by Gaussian curves with a spectral width (FWHM) of 7.5 nm. This width was chosen to match the left side of the experimental spectrum as shown in Fig. 7 and is typical for atomic emission lines in solid helium. The amplitudes of the curves are given by the calculated Franck-Condon factors.

The calculated emission band has its peak at 1022 nm, whereas the experimental band peaks at 1042 nm. This shift of 20 nm can be attributed either to the interaction of the molecule with the helium matrix, or to the imprecision of the theoretical molecular potentials. Atomic emission lines in solid and liquid He are known to be shifted by 10-15 nm towards shorter wavelengths, and to show an increase of this shift with the increase of He pressure. However, our observations of the molecular fluorescence band discussed here show that its spectral position and its lineshape do not depend on pressure, which leads us to conclude that the observed wavelength is close to the one of the free molecule. As the ground-state potential curve is very well known from theory and experiments [3, 29], one therefore has to suspect imprecisions of the  $(1)^3\Pi_u$  potential curve to be responsible for the 20 nm shift. There are no detailed spectroscopic studies of this state. Only the mutual perturbation of the  $A^1\Sigma_u$  and  $(1)^3\Pi_u$  states in the vicinity of their crossing point at  $5.1 \text{ \AA}$  was studied [30]. The observed fluorescence spectrum (dots) and the calculated band shifted by 20 nm (curve 1), are compared in Fig. 7, after scaling the amplitude of the calculated spectrum. The 20 nm shift suggests that the depth of the calculated potential well is underestimated by  $190 \text{ cm}^{-1}$ .

The observed emission spectrum has a pronounced asymmetry. It may result from the overlap of several (two) vibronic transitions, as discussed above. However, when each component is modelled by a symmetric Gaus-

band	label	$\lambda_{theor}$	$\lambda_{exper}$
$X^1\Sigma_g \rightarrow A^1\Sigma_u$	a	878	842
$(1)^3\Sigma_u \rightarrow (1)^3\Pi_g$	b	735	742
$X^1\Sigma_g \rightarrow B^1\Pi_u$	c	664	653
$(1)^3\Sigma_u \rightarrow (3)^1\Sigma_g$	d	623	622
$(1)^3\Sigma_u \rightarrow (2)^3\Sigma_g$	e	590	580
$(1)^3\Sigma_u \rightarrow (2)^3\Pi_g$	e	586	580
$(1)^3\Sigma_u \rightarrow (3)^3\Sigma_g$	f	507	524
$X^1\Sigma_g \rightarrow (2)^1\Sigma_u$	g	477	445
$X^1\Sigma_g \rightarrow (2)^1\Pi_u$	g	464	445
$(1)^3\Sigma_u \rightarrow (2)^3\Sigma_u$	i	670	649
$X^1\Sigma_g \rightarrow (3)^1\Sigma_g$	j	505	493

TABLE I: Calculated and measured wavelengths of  $\text{Rb}_2$  absorption bands (in nm). The second column shows the labels of the corresponding peaks in Fig. 3.

sian curve, the resulting asymmetry is smaller than that of the experimental spectrum (see Fig. 7). This discrepancy can be reduced if one shifts the minimum of the excited state potential with respect to that of the ground state. Curve 2 in Fig. 7 was obtained by shifting this potential curve by  $0.12 \text{ \AA}$  towards larger interatomic distances and yields a better agreement with the experimental data. The alternative interpretation of the discrepancy between the measured and calculated emission spectra is presented below, in Sec. III D.

### C. Molecular absorption spectrum

When comparing the calculated Franck-Condon factors of the absorption bands shown in Fig. 3(b) to the experimentally measured spectra of Fig. 3(a) one can identify all observed bands. The calculated wavelengths of the band maxima are presented in the third column of Table III C. The relative intensities can not be predicted by our model which does not consider the transition dipole moments. We have fitted the experimental spectra with Gaussian curves. The results of the fits are shown in Fig. 3(a) as solid lines and the positions of the band maxima are collected in the fourth column of Table III C.

The strongest absorption band at 842 nm (band "a" in Fig. 3(a)) belongs to the  $X^1\Sigma_g \rightarrow A^1\Sigma_u$  transition. The experimentally measured absorption band is blueshifted with respect to the calculated one by 35 nm. This shift can again be attributed either to the influence of the He-matrix, or to an uncertainty in the excited state potential curve. The band at 740 nm (band "b" in Fig. 3(a)) is assigned to the  $(1)^3\Sigma_u \rightarrow (1)^3\Pi_g$  transition. Both the excited and the ground state have very shallow potential wells and therefore the transition wavelength is very close to that of the atomic  $\text{D}_2$  absorption line (the red component of the doublet "h" in Fig. 3(c)).

Another strong absorption band is observed at 653 nm (band "c" in Fig. 3(a)). We identify it as the



$X^1\Sigma_g \rightarrow B^1\Pi_u$  band. The calculated band position is at 664 nm. The potential curves of the involved states are well known from experiments [29, 31]. The blueshift due to the interaction with the He-matrix is 11 nm, significantly smaller than that of the atomic lines and of the  $X^1\Sigma_g \rightarrow A^1\Sigma_u$  band.

The weak absorption band labelled "d" in Fig. 3(a) lies in a spectral region in which no allowed molecular transitions exist. Its wavelength strongly depends on the helium pressure. We suppose that this band (at 622 nm) is due to the forbidden transition  $(1)^3\Sigma_u \rightarrow (3)^1\Sigma_g$  from the triplet ground-state.

The observed absorption band at 580 nm (peak "e" in Fig. 3) is a superposition of two allowed triplet-triplet bands:  $(1)^3\Sigma_u \rightarrow (2)^3\Sigma_g$  and  $(1)^3\Sigma_u \rightarrow (2)^3\Pi_g$ . None of these states has been studied experimentally before. The calculated wavelengths of both transitions are longer than the experimental one by 6 and 10 nm respectively.

The absorption band at 525 nm (peak "f" in Fig. 3(a)) can be attributed to another triplet-triplet system:  $(1)^3\Sigma_u \rightarrow (3)^3\Sigma_g$ . The calculated position of this band is at 507 nm, *i. e.* the interaction with the matrix shifts it to the red, unlike all other observed bands.

The narrow band at 445 nm (peak "g" in Fig. 3(a)) can be assigned to allowed transitions from the singlet ground state. The  $X^1\Sigma_g \rightarrow (2)^1\Sigma_u$  and  $X^1\Sigma_g \rightarrow (2)^1\Pi_u$  bands with calculated wavelengths of 477 and 465 nm respectively are good candidates to explain this band.

#### D. Speculation about the formation of a molecular $\text{Rb}_2^*\text{He}_N$ exciplex

We have shown above that every observed excitation of the  $\text{Rb}_2$  dimer finally leads to a population of the  $(1)^3\Pi_u$  state. The laser-excited states do not fluoresce at the excitation wavelength, nor do they emit fluorescence in the near (red or blue) vicinity of the excitation wavelength as atoms, *e. g.*, typically do. The quenching of all upper states thus seems to occur on a time scale which is much shorter than their radiative lifetimes. This deexcitation proceeds via a direct or a cascade-like radiationless transition or via transitions emitting far-infrared light, which is not accessible by our spectrometer. Only the final metastable state  $(1)^3\Pi_u$ , perturbed by the interaction with the surrounding He, lives long enough to emit fluorescence with a lifetime of 45  $\mu\text{s}$ .

Besides this long lifetime we have observed an intriguingly long (15  $\mu\text{s}$ ) rise-time of the fluorescence signal which indicates that the fluorescing state is populated via some intermediate metastable level. This state must lie below the  $A^1\Sigma_u$  state, the lowest lying level after whose excitation one observes the 1042 nm fluorescence. In Fig. 6 one sees that no such state exists in the free  $\text{Rb}_2$  molecule.

For this reason we tentatively explain the observation in terms of a relatively slow conformational change of the system formed by the metastable  $\text{Rb}_2(^3\Pi_u)$  molecule and

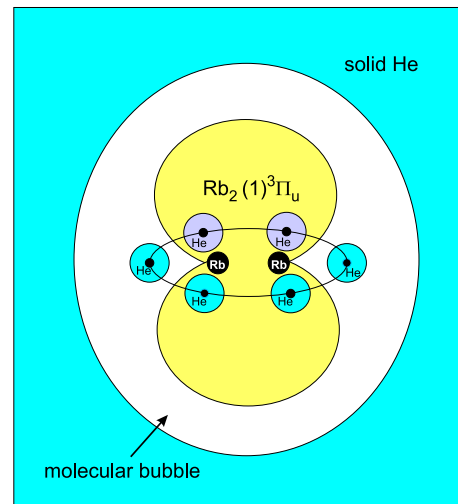


FIG. 8: Structure of the molecular  $\text{Rb}_2^*\text{He}_N$  exciplex in which several He atoms from the interface of the molecular bubble produce a bound or quasi-bound state with the rotationally quenched metastable  $\text{Rb}_2$  ( $(1)^3\Pi_u$ ) molecule. This structure is proposed for explaining the puzzling time-dependence of the molecular fluorescence.

the surrounding helium atoms (molecular bubble). The quantitative modelling of the interaction between the defect molecule and the He crystal is beyond the scope of the present paper. However, such a theoretical study was reported recently [32] for the hydrogen molecule embedded in liquid He. For the metastable  $c^3\Pi_u$  state which is analogous to the  $(1)^3\Pi_u$  state of  $\text{Rb}_2$  the authors of [32] suggest an exciplex structure consisting of several He atoms bound around the waist of the dumbbell-shaped molecular orbital of  $\text{H}_2$ . This structure closely resembles that of  $\text{Cs}(6P_{1/2})\text{He}_7$  and  $\text{Rb}(5P_{1/2})\text{He}_6$  exciplexes observed in our recent experiments [19, 21] in solid He, it is shown schematically in Fig. 8. Here we suggest that a similar molecular exciplex  $\text{Rb}_2^*\text{He}_N$  could be formed by the  $(1)^3\Pi_u$  state of the  $\text{Rb}_2$  molecule in solid He.

The metastable state of the dimer is prepared in a relatively large molecular bubble. In order to leave the bubble surface and to move towards the dimer, the He atoms have to tunnel through a potential barrier. The tunnelling time may be as long as a few microseconds, which would explain the slow onset of the fluorescence. The perturbation of the dimer by the bound He atoms lifts the selection rule that forbids the radiative transition to the singlet ground-state. Unlike the atomic exciplexes studied in [19, 21], the suggested molecular exciplex has a very long life-time and its emission spectrum is very similar to that of a free  $\text{Rb}_2$  molecule. The interaction between the elliptical orbital of the  $X^1\Sigma_g$  ground state of  $\text{Rb}_2$  and the attached He atoms is repulsive and shifts the ground state towards higher energies. It is responsible for the redshift of the measured emission spectrum whose pressure-independence remains an open question. After fluorescing the exciplex dissociates and the He atoms re-

turn to the bubble interface. The 1042 nm fluorescence thus does not originate from the metastable  $(1)^3\Pi_u$  state directly, but rather from an exciplex formed by that state.

### E. Photodissociation spectrum

The excitation spectrum for atomic emission at 760 nm is presented in Fig. 3(c). Only the doublet labelled "h" represents absorption by individual Rb atoms ( $D_1$  and  $D_2$  absorption lines). The peaks: "d", "e", "i", and "j" represent photodissociation lines of the  $\text{Rb}_2$  molecule. Three of them ("d", "e", and "i") lie very close to the molecular absorption bands discussed in the previous section, while the peak "j" has no analog in the absorption spectrum of Fig. 3(a).

The calculated Franck-Condon factors for the relevant molecular bands are shown in Fig. 3(d). The lineshapes of the bound-free transition  $(1)^3\Sigma_u \rightarrow (2)^3\Sigma_u$  (peak "i") and of the bound-free part of the  $(1)^3\Sigma_u \rightarrow (1)^3\Pi_g$  band (peak "b") are calculated based on a standard adiabatic line-broadening theory [33] as the Fourier transform of the autocorrelation function

$$C(\tau) = \exp\left\{-\int (1 - \exp[-i\Delta\nu(r)\tau])\Psi_g^{(0)}(r)^2 dr\right\}, \quad (4)$$

where  $\Delta\nu(r)$  represents the transition energy corresponding to the interatomic separation  $r$ . Only the bound-free part of the  $(1)^3\Sigma_u \rightarrow (1)^3\Pi_g$  band is shown in Fig. 3(d), whereas the bound-bound components of this band are represented in Fig. 3(b) by their Franck-Condon factors.

The blue component of the atomic absorption doublet "h" ( $D_2$  resonance line) overlaps with the molecular  $(1)^3\Sigma_u \rightarrow (1)^3\Pi_g$  absorption band ("b" in Fig. 3(a)). As can be seen from Fig. 6, the position of the minimum (6.1 Å) of the shallow potential well of the triplet ground-state is much larger than that of the  $(1)^3\Pi_g$  state. The Condon point of the excited state is right at the top of the potential barrier. Excitations occurring at smaller distances thus populate vibrational states which rapidly relax towards the bottom of the potential well with subsequent radiationless transitions to lower-lying electronic states, and finally to the  $(1)^3\Pi_u$  state. On the other hand, absorption at larger internuclear distances populates the right side of the  $(1)^3\Pi_g$  potential barrier which results in the dissociation of the molecule into a  $5S$  ground-state atom and an atom in the excited  $5P$  state. This dissociation channel cannot be distinguished from the purely atomic absorption-emission cycle in our experiments. A similar competition between quenching and dissociation of the  $(1)^3\Pi_g$  state was observed in experiments on potassium dimers attached to helium nanodroplets [10, 13], where the atomic absorption lines and the molecular  $(1)^3\Sigma_u \rightarrow (1)^3\Pi_g$  band were resolved. In those experiments the quenching of the laser-excited  $(1)^3\Pi_g$  state of  $\text{K}_2$  resulted in fluorescence

at the two allowed singlet-singlet transitions, whose upper states lie below the  $(1)^3\Pi_g$  state:  $A^1\Sigma_u \rightarrow X^1\Sigma_g$  and  $B^1\Pi_u \rightarrow X^1\Sigma_g$ . The fast desorption of the excited molecule from the surface of the droplet prevented the population of the metastable  $(1)^3\Pi_g$  state to be observed in that study.

The photodissociation band "i" has almost the same wavelength as the  $X^1\Sigma_g \rightarrow B^1\Pi_u$  band in Fig. 3(a) (labelled "c"). However, the Condon point of the  $B^1\Pi_u$  potential lies well below the dissociation limit, and hence no photodissociation is expected. We therefore attribute the peak "i" to a dissociation of the dimer following absorption from the triplet ground-state. The only band that has a corresponding wavelength is the forbidden  $(1)^3\Sigma_u \rightarrow (2)^3\Sigma_u$  transition at 670 nm. The excited state is strongly repulsive and the shift due to the interaction with the matrix has the same sign as for all other bands and a magnitude of 20 nm. The photodissociation at the wavelength close to the  $X^1\Sigma_g \rightarrow B^1\Pi_u$  band of  $\text{Rb}_2$  was observed in an experiment with He-nanodroplets [12]. The authors of [12] interpret it as either the forbidden  $(1)^3\Sigma_u \rightarrow (2)^3\Sigma_u$  transition that becomes allowed due to the perturbation of the  $\text{Rb}_2$  molecule by the matrix, or as the dissociation of a  $\text{Rb}_3$  molecule.

The photodissociation peak at 625 nm overlaps with the peak "d" of Fig. 3(a), and therefore we assign it to the same forbidden  $(1)^3\Sigma_u \rightarrow (3)^1\Sigma_g$  transition. The potential curve of the  $(3)^1\Sigma_g$  state below the Condon point is crossed by the repulsive  $(2)^3\Sigma_u$  state and by the strongly bound  $(2)^3\Sigma_g$  state. The transition to the former results in the dissociation of the dimer, while the latter is connected by an allowed transition to the metastable  $(1)^3\Pi_u$  state which fluoresces at 1042 nm.

Using the same arguments we can assign the asymmetric photodissociation band at 590 nm (peak "e" of Fig. 3(c)) to a superposition of the  $(1)^3\Sigma_u \rightarrow (2)^3\Sigma_g$  and  $(1)^3\Sigma_u \rightarrow (2)^3\Pi_g$  transitions. The photodissociation is due to the crossing of the  $(2)^3\Sigma_g$  state with the repulsive  $(2)^3\Sigma_u$  state at  $R=5.5$  Å, below the Condon point.

Finally, the band peaked at 493 nm (peak "j" in Fig. 3(c)) produces no molecular fluorescence but only photodissociation. It can be assigned to one of the three forbidden transitions from the singlet ground-state, viz.,  $X^1\Sigma_g \rightarrow (3)^1\Sigma_g$  (505 nm),  $X^1\Sigma_g \rightarrow (2)^3\Pi_u$  (496 nm), or  $X^1\Sigma_g \rightarrow (2)^3\Sigma_u$  (488 nm). The upper state of the last transition is repulsive, while the upper states of the first two transitions cross it below their Condon points and may thus also populate it.

### F. Photodissociation vs molecular emission at the phase transition

Here we suggest a speculative qualitative interpretation of the changes in the fluorescence spectrum at the solid-liquid phase transition. The fluorescence at 1042 nm following the excitation at 650 nm disappears during the transition to the liquid phase because the up-



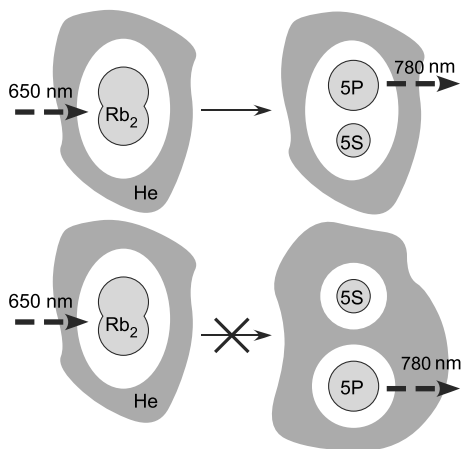


FIG. 9: Possible final bubble configurations following dissociation of the  $\text{Rb}_2$  dimer by absorption of 650 nm light. The situation shown on top is energetically favored. Experimental evidence that the upper graph describes the dissociation process comes from the fact that the atomic fluorescence line emitted after photodissociation is less shifted than the well studied emission from the atomic bubble (bottom graph).

per  $B^1\Pi_u$  state becomes less perturbed by the surrounding helium and the rate of radiationless transition to the metastable  $(1)^3\Pi_u$  state drops below that of the allowed radiative transition  $B^1\Pi_u \rightarrow X^1\Sigma_g$ . This emission is difficult to detect experimentally because of a very strong background from scattered laser light at 650 nm. Nonetheless the red wing of this band appears in the experimental spectra close to the atomic doublet. On the other hand, the photodissociation at 650 nm is much less sensitive to changes in the helium density because the dissociating state is populated directly by absorption and involves no radiationless transition.

The absorption at 580 nm populates the states  $(2)^3\Sigma_g$  and  $(2)^3\Pi_g$  which themselves do not dissociate but which have allowed radiative transitions to the metastable  $(1)^3\Pi_u$  state and thus do fluoresce at 1042 nm. In consequence, a reduction of the helium density results in a suppression of the photodissociation due to matrix induced mixing with dissociative states, while the metastable state is still efficiently populated and thus emits fluorescence.

The systematic difference of the spectral shifts of the atomic emission lines following excitation via different channels (atomic absorption at 760 nm or photodissociation at 650 nm) suggests that the presence of the second (ground-state) Rb atom (resulting from the dissociation) reduces the perturbation imposed by the surrounding He on the fluorescence emitting Rb atom. The bubble model [18, 25] successfully predicts the shifts of the resonance lines of Rb and Cs bubbles in liquid and solid He. As the electronic density of the excited  $P$  state in the alkali occupies a larger volume than its ground state, it has a larger overlap with the surrounding He. Due to the Pauli

repulsion, this overlap results in a shift of the atomic levels towards higher energies. Because of the larger shift of the excited state the transition becomes blue shifted.

Based on the bubble model we suggest the following qualitative interpretation of the observed lineshifts at the phase transition. The  $\text{Rb}_2$  dimer forms a molecular bubble whose shape reflects the symmetry of the molecule's electronic configuration. The photodissociation of  $\text{Rb}_2$  does not result in the formation of two independent atoms occupying each an individual bubble, but the two Rb atoms, separated by several Å, will rather reside in a single large helium bubble (Fig. 9). It is not clear a priori whether this diatomic bubble configuration is energetically favored over the situation, in which atoms reside in individual bubbles. Because of the larger average distance of the first He solvation shell this molecular bubble will perturb the atomic levels to a lesser extent than the smaller monoatomic bubble (studied in [18, 25]) and could therefore explain the smaller spectral shifts of the observed emission lines.

#### IV. SUMMARY

We have presented results of laser-induced fluorescence experiments in solid He doped by laser ablation from a metallic rubidium target. We have observed for the first time fluorescence from Rb atoms and from  $\text{Rb}_2$  dimers in solid He. Atomic emission was observed after atomic excitation as well as after excitation of photodissociating states in the  $\text{Rb}_2$  molecule. In the latter case the atomic emission lines are less perturbed than after direct atomic excitation, a fact which we attribute to emission from diatomic bubbles.

Absorption and emission bands of  $\text{Rb}_2$  were studied in the visible and near infrared domains. All absorption and photodissociation bands in this range could be assigned by comparison with calculated Franck-Condon factors. No emission from any of the allowed transitions of the free  $\text{Rb}_2$  molecule could be observed in the investigated spectral range. At the same time we found a large number of absorption bands which all lead to emission of fluorescence on the forbidden transition from the metastable  $(1)^3\Pi_u$  state to the ground state. The emitting state was found to have a lifetime of 45  $\mu\text{s}$  and a formation time of 15  $\mu\text{s}$ . We interpret this feature by proposing that the metastable state forms (on a time scale of 15  $\mu\text{s}$ ) a  $\text{Rb}_2(^3\Pi_u)\text{He}_N$  molecular exciplex, which then decays with a lifetime of 45  $\mu\text{s}$ .

#### Acknowledgments

This work was supported by grant No. 200020-103864 of the Schweizerischer Nationalfonds.

- 
- [1] D. L. Drummond and L. A. Schlie, *J. Chem. Phys.* **65**, 2116 (1976).
- [2] G. Pichler, S. Milosevic, D. Veza, and D. Vukicevic, *J. Phys. B* **16**, 4633 (1983).
- [3] C. Amiot, *J. Chem. Phys.* **93**, 8591 (1990).
- [4] Y. Lee, Y. Yoon, S. J. Baek, D.-L. Joo, J. Ryu, and B. Kim, *J. Chem. Phys.* **113**, 2116 (2000).
- [5] A. Fioretti, C. Amiot, C. M. Dion, O. Dulieu, M. Mazzoni, G. Smirne, and C. Gabbanini, *Eur. Phys. J. D* **15**, 189 (2001).
- [6] R. F. Gutterres, C. Amiot, A. Fioretti, C. Gabbanini, M. Mazzoni, and O. Dulieu, *Phys. Rev. A* **66**, 024502 (2002).
- [7] T. Bergeman, A. J. Kerman, J. M. Sage, S. Sainis, and D. DeMille, *Eur. Phys. J. D* **31**, 179 (2004).
- [8] W. C. Stwalley, *Eur. Phys. J. D* **31**, 221 (2004).
- [9] S. Azizi, M. Aymar, and O. Dulieu, *Eur. Phys. J. D* **31**, 195 (2004).
- [10] J. Higgins, C. Callegari, J. Reho, F. Stienkemeier, W. E. Ernst, M. Gutowski, and G. Scoles, *J. Phys. Chem.* **102**, 4952 (1998).
- [11] O. Bunermann, M. Mudrich, M. Weidemuller, and F. Stienkemeier, *J. Chem. Phys.* **121**, 8880 (2004).
- [12] F. R. Bruhl, R. A. Miron, and W. E. Ernst, *J. Chem. Phys.* **115**, 10275 (2001).
- [13] J. Reho, J. Higgins, and K. Lehmann, *Faraday Discuss.* **118**, 33 (2001).
- [14] Y. Takahashi, K. Sano, T. Kinoshita, and T. Yabuzaki, *Phys. Rev. Lett.* **71**, 1035 (1993).
- [15] T. Welker and T. P. Martin, *J. Chem. Phys.* **70**, 5683 (1979).
- [16] M. Gross and F. Spiegelmann, *J. Chem. Phys.* **108**, 4148 (1998).
- [17] B. Gervais, E. Giglio, E. Jacquet, A. Ipatov, P. G. Reinhard, F. Fehrer, and E. Siraud, *Phys. Rev. A* **71**, 015201 (2005).
- [18] S. Kanorsky, A. Weis, M. Arndt, R. Dziewior, and T. W. Hänsch, *Z. Phys. B* **98**, 371 (1995).
- [19] P. Moroshkin, A. Hofer, D. Nettels, A. Hofer, S. Ulzega, and A. Weis, *J. Chem. Phys.* **124**, 024511 (2006).
- [20] T. Eichler, R. Müller-Siebert, D. Nettels, S. I. Kanorsky, and A. Weis, *Phys. Rev. Lett.* **88**, 123002 (2002).
- [21] A. Hofer, P. Moroshkin, S. Ulzega, and A. Weis, to be published.
- [22] T. Kinoshita, K. Fukuda, T. Matsuura, and T. Yabuzaki, *Phys. Rev. A* **53**, 4054 (1996).
- [23] S. Kanorsky, M. Arndt, R. Dziewior, A. Weis, and T. W. Hänsch, *Phys. Rev. B* **49**, 3645 (1994).
- [24] J. H. Vignos and H. A. Fairbank, *Phys. Rev. Lett.* **6**, 265 (1961).
- [25] T. Kinoshita, K. Fukuda, Y. Takahashi, and T. Yabuzaki, *Phys. Rev. A* **52**, 2707 (1995).
- [26] S. J. Park, S. W. Suh, Y. S. Lee, and G. H. Jeung, *J. Mol. Spectr.* **207**, 129 (2001).
- [27] F. Spiegelmann, D. Pavolini, and J. P. Daudey, *J. Phys. B* **22**, 2465 (1989).
- [28] J. Helbing, M. Chergui, and A. Haydar, *J. Chem. Phys.* **113**, 3621 (2000).
- [29] C. Amiot, P. Crozet, and J. Verges, *Chem. Phys. Lett.* **121**, 390 (1985).
- [30] B. Zhang, N. Gador, and T. Hansson, *Phys. Rev. Lett.* **91**, 173006 (2003).
- [31] C. Amiot and J. Verges, *Chem. Phys. Lett.* **274**, 91 (1997).
- [32] T. Kiljunen, L. Lehtovaara, H. Kuntu, and J. Eloranta, *Phys. Rev. A* **69**, 012506 (2004).
- [33] N. Allard and J. Kielkopf, *Rev. Mod. Phys.* **54**, 1103 (1982).